

Research Paper

# A Novel Inherently Radiopaque Bead for Transarterial Embolization to Treat Liver Cancer – A Pre-clinical Study

Rafael Duran<sup>1,2</sup>, Karun Sharma<sup>3</sup>, Matthew R. Dreher<sup>4</sup>, Koorosh Ashrafi<sup>5</sup>, Sahar Mirpour<sup>1</sup>, MingDe Lin<sup>6</sup>, Ruediger E. Schernthaler<sup>1,2</sup>, Todd R. Schlachter<sup>1,2</sup>, Vania Tacher<sup>1</sup>, Andrew L. Lewis<sup>5</sup>, Sean Willis<sup>5</sup>, Mark den Hartog<sup>7</sup>, Alessandro Radaelli<sup>7</sup>, Ayele H. Negussie<sup>8</sup>, Bradford J. Wood<sup>8</sup>, Jean-François H. Geschwind<sup>1,2</sup>✉

1. Russell H. Morgan Department of Radiology and Radiological Science, Division of Vascular and Interventional Radiology, Johns Hopkins Hospital, Baltimore, MD, USA
2. Department of Diagnostic Radiology and Imaging Science, Yale University School of Medicine, New Haven, CT, USA
3. Department of Diagnostic Imaging and Radiology, Children's National Medical Center, Washington, DC, USA
4. Biocompatibles Inc, Oxford, CT, USA
5. Biocompatibles UK Ltd, a BTG International group company, Farnham, Surrey, United Kingdom
6. U/S Imaging and Interventions (UII), Philips Research North America, Briarcliff Manor, NY, USA
7. iXR, Philips Healthcare, Best, The Netherlands
8. Center for Interventional Oncology, Radiology and Imaging Sciences, Clinical Center, National Institutes of Health, Bethesda, MD, USA

✉ Corresponding author: Jean-François H. Geschwind, MD, Chairman of Department of Diagnostic Radiology, Yale University School of Medicine, Department of Diagnostic Radiology, Chairman's Office, 330 Cedar Street, TE 2-230, New Haven, CT 06520, Phone: +1 (203) 785-6938; Fax: +1 (203) 785-3024; Email: jeff.geschwind@yale.edu

© 2015 Ivyspring International Publisher. Reproduction is permitted for personal, noncommercial use, provided that the article is in whole, unmodified, and properly cited. See <http://ivyspring.com/terms> for terms and conditions.

Received: 2015.07.04; Accepted: 2015.08.19; Published: 2016.01.01

## Abstract

**Purpose:** Embolotherapy using microspheres is currently performed with soluble contrast to aid in visualization. However, administered payload visibility diminishes soon after delivery due to soluble contrast washout, leaving the radiolucent bead's location unknown. The objective of our study was to characterize inherently radiopaque beads (RO Beads) in terms of psychomechanical properties, deliverability and imaging visibility in a rabbit VX2 liver tumor model.

**Materials and Methods:** RO Beads, which are based on LC Bead® platform, were compared to LC Bead. Bead size (light microscopy), equilibrium water content (EWC), density, X-ray attenuation and iodine distribution (micro-CT), suspension (settling times), deliverability and *in vitro* penetration were investigated. Fifteen rabbits were embolized with either LC Bead or RO Beads + soluble contrast (iodixanol-320), or RO Beads+dextrose. Appearance was evaluated with fluoroscopy, X-ray single shot, cone-beam CT (CBCT).

**Results:** Both bead types had a similar size distribution. RO Beads had lower EWC (60-72%) and higher density (1.21-1.36 g/cc) with a homogeneous iodine distribution within the bead's interior. RO Beads suspension time was shorter than LC Bead, with durable suspension (>5 min) in 100% iodixanol. RO Beads ≤300 μm were deliverable through a 2.3-Fr microcatheter. Both bead types showed similar penetration. Soluble contrast could identify target and non-target embolization on fluoroscopy during administration. However, the imaging appearance vanished quickly for LC Bead as contrast washed-out. RO Beads+contrast significantly increased visibility on X-ray single shot compared to LC Bead+contrast in target and non-target arteries ( $P=0.0043$ ). Similarly, RO beads demonstrated better visibility on CBCT in target arteries ( $P=0.0238$ ) with a trend in non-target arteries ( $P=0.0519$ ). RO Beads+dextrose were not sufficiently visible to monitor embolization using fluoroscopy.

---

**Conclusion:** RO Beads provide better conspicuity to determine target and non-target embolization compared to LC Bead which may improve intra-procedural monitoring and post-procedural evaluation of transarterial embolization.

---

Key words: VX2, Embolization, Hepatocellular carcinoma, TACE, radiopaque beads

## Introduction

Image-guided catheter-directed embolization is a mainstay of interventional radiology. Typical procedures include uterine artery embolization, control of inoperable hemorrhage, devascularization of highly vascular tumors prior to resection, transarterial embolization (TAE) and chemoembolization (TACE) of malignant liver neoplasms. Embolic agents may include liquid, particulate and mechanical devices deployed at a specific location, which may be temporary or permanent. The choice of embolic agent depends on the therapeutic intent, and recently microspherical particulates (commonly referred to as beads) have emerged as a popular device for a range of embolo-therapeutic applications [1]. Soluble contrast medium is mixed with the beads to aid in visualization of embolic delivery into the targeted tissue and also to monitor unintentional reflux into non-target blood vessels. Success of embolization is determined by monitoring antegrade flow of soluble contrast medium to reach the desired flow-based procedural endpoint of reduced or nearly static blood flow [2]. Soluble contrast retention in the tumor and/or lack of tumor contrast enhancement due to the embolization, monitored with cone-beam computed tomography (CBCT) or multidetector CT (MDCT), may be employed to indicate coverage or completeness of treatment and to predict response and recurrence [3-6]. However, the true bead location is unknown and only inferred from indirect and temporary signs as soluble contrast medium washes out [3-6].

A clinical need exists to directly visualize the embolic material in order to assess the completeness of the target tissue embolization for efficacy as well as unintentional embolization of non-target tissue for safety. For example, in the embolization of hepatocellular carcinoma, the goal is to completely embolize the tumor while avoiding non-target tissue embolization [2]. A radiopaque bead may provide additional procedural value by improving the visualization of target and non-target embolization compared to soluble contrast medium alone. This unmet clinical need has motivated the development of various radiopaque embolic agents using processes such as chemical precipitation, encapsulation and chemical attachment of radiopaque species. Previous publications described the preparation of various of radiopaque beads based on many polymers including

poly(methylmethacrylate) (PMMA), poly(hydroxyethylmethacrylate), silicone and polyvinyl alcohol (PVA) that were rendered radiopaque using processes such as precipitation of barium sulphate or incorporation of tantalum powder within the polymer matrix and reaction with iodine-containing compounds such as iothalamic acid and 3-acetylamino-2,4,6-triiodobenzoyl chloride [7-11]. There are numerous recent examples of imageable beads that are visualized by X-ray (e.g. fluoroscopy and CT) [12-16], magnetic resonance imaging [17-21], or both [22, 23]. However, these imageable beads have not obtained widespread clinical adoption.

One challenge faced is that many of the imageable embolization particles often suffer from difficulty in handling and administration due to their increased density, aggregation potential and insufficient imaging visibility. Moreover, these attributes are often in competition with each other. For example, greater image visibility may be achieved with a higher concentration of radiopaque material but this increases the density and may lead to diminished handling due to rapid sedimentation. The goal of our study was to characterize the physicomaterial properties, deliverability and imaging visibility of a novel inherently radiopaque bead (RO Bead) formulation based upon the clinically used LC Bead® to treat liver cancer.

## Materials and Methods

There were two stages of studies conducted. The first was bench-top experiments to characterize physicomaterial properties of RO Beads, especially in comparison to radiolucent beads. The second portion of the study was an *in vivo* X-ray visualization experiment in a rabbit VX2 liver tumor model. Details of the study are below.

### Bench-top Experiments

#### Radiopaque Beads Synthesis

The method for the preparation of LC Bead® (Biocompatibles UK Ltd., Farnham, UK) has been described in detail elsewhere [24]. Briefly, the beads were produced using a PVA-based macromer. The macromer was synthesized by the acid-catalyzed reaction of N-acryloyl-aminoacetaldehyde dimethylacetal (NAAADA) with the 1,3 diol units on the PVA backbone to form a stable cyclic acetal structures with

pendent reactive acrylamide groups. The macromer was used in an inverse suspension free-radical copolymerization with 2-acrylamido-2-methylpropanesulfonate sodium salt (AMPS). The aqueous macromer/monomer mixture was suspended in butyl acetate and stabilised by cellulose acetate butyrate to prevent coagulation. Potassium persulfate was used as one half of a redox initiator couple, which is present in the aqueous phase. The stirred mixture was heated to 60°C and then tetramethylethylenediamine (TMEDA, the other component of the redox couple) was added to the oil phase, where upon polymerization was initiated and a water-swollen crosslinked network formed. After the polymerization was complete the beads were dried by washing in acetone and drying in an oven at 40°C overnight to form a free-flowing powder [24]. PVA-AMPS beads were originally developed from contact lens technology and are thus inherently optically transparent and biocompatible. These beads are tinted blue using a reactive dye (Reactive Blue 4, RB4) to enable visualization of the bead suspension to make for easier handling (Figure 1). A novel process was developed in which the blue tinting step was replaced by an alternative reaction to attach a radiopaque moiety (triiodinated benzyl) to the preformed hydrogel (Figure 1). In order to couple the radiopaque compound to the polymer backbone, the beads in dimethyl sulfoxide (DMSO) were reacted with 2,3,5-triiodobenzaldehyde in an acid-catalyzed reaction under nitrogen with

stirring, to form stable cyclic acetal linkages with pendent triiodobenzyl moieties. Consumption of the aldehyde was monitored using high-performance liquid chromatography (HPLC) and once complete, the reaction was filtered. The cake of beads was washed thoroughly with copious amounts of DMSO and then water, until free of unreacted aldehyde as determined by HPLC.

### Bead Physical Property Characterization

LC Bead and RO Bead size was determined by forming a monolayer of beads within a petri dish. Bead images were acquired at x10 magnification with an Olympus BX50 microscope equipped with a ColorView III camera and sizing was performed manually using the sizing tool provided in the ANALYSIS software package (Soft Imaging Systems GmbH, Berlin, Germany). A population of at least 200 microspheres was chosen at random throughout the dish.

Bead density was determined by using Eppendorf tubes containing a plastic insert with a 5 µm pore size at the bottom of the insert. First the insert was wetted with saline and then centrifuged at 1,200 g for 1 minute. The weight of the wet insert was recorded. Beads were added to the insert and the centrifugation and weighing steps were repeated. The bead volume was then measured by displacement of saline in a graduated cylinder and the density of wet beads determined (mass/volume, N=3).

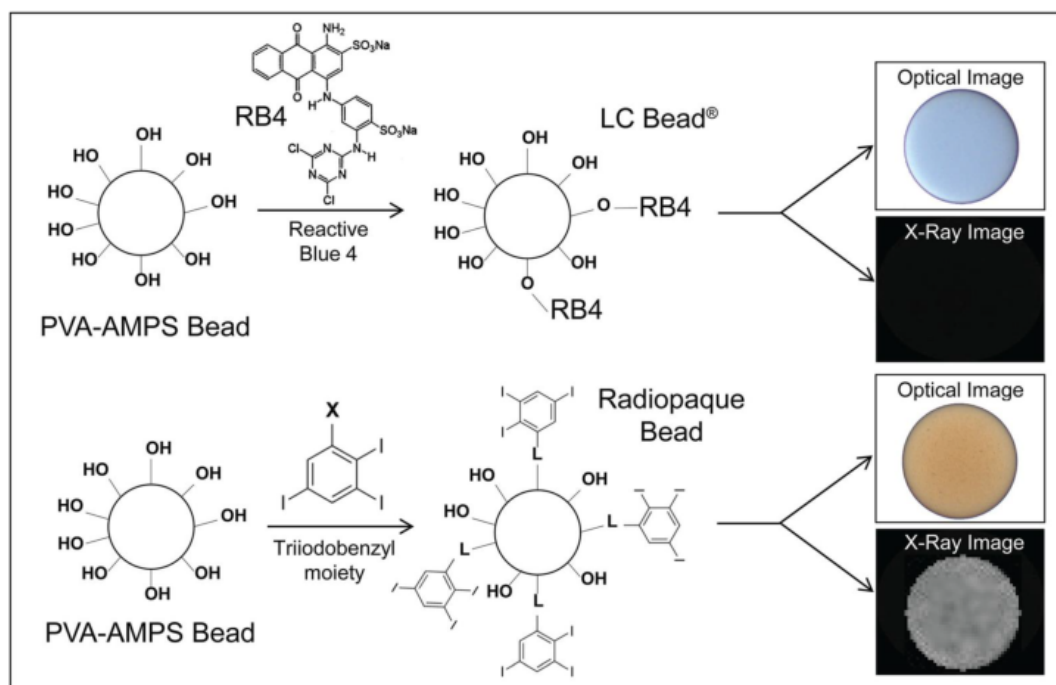


**Figure 1:** Comparison of LC Bead and Radiopaque LC Bead (RO Bead) dye attachment. Acrylamido polyvinyl alcohol-co-acrylamido-2-methylpropane sulfonate hydrogel (PVA-AMPS) beads are reacted with Reactive Blue 4 (RB4) to make LC Bead visible (blue) to the user. RB4 is substituted with a triiodobenzyl moiety via a linker (L) for RO Beads which imparts a slight yellow color and importantly renders them visible on X-ray.

To calculate the equilibrium water content (EWC), between 0.2 and 0.3 mL of sedimented beads were washed 3x with 10 mL deionized water and placed on a shaker plate at 250 rpm for 5 minutes in order to remove residual salts present in the packing solution (beads are supplied in vials hydrated in physiologically buffered saline). The washed beads were then transferred to a pre-weighed aluminum plate using a Pasteur pipette and minimum amount of deionized water to aid complete transfer of beads. Excess water was removed by first using a Pasteur pipette followed by filter paper gently pressed against the beads to remove residual surface water. The mass of the plate with wet beads was then obtained. The aluminum plates containing beads were then transferred to a vacuum oven and the samples were allowed to dry at a pressure of 50-100 mBar and at 50°C. After 12 hours, the aluminum plates containing the dried beads were weighed to calculate EWC. The dried beads were then transferred to clean dry vials, stoppered and crimped with aluminum caps. These samples were then subjected to elemental analysis for iodine (MEDAC Ltd, Chobham, UK) to calculate iodine concentration (N=3). Iodine concentration was expressed per true bead volume (i.e. the amount of iodine within the bead volume) and per sedimented bead volume. The iodine concentration per true bead volume is greater due to the imperfect tessellation of packed beads with presence of water around the sedimented beads.

Elastic modulus was calculated with a UMIS 2000 nanoindentation system (CSIRO Instruments, Lindfield NSW, Australia) operated by IBIS software (Force range 0.01-45 mN; displacement range 1 nm-100 µm). Individual beads were selected using the optical microscope on the UMIS instrument and their diameters measured to the nearest 5 µm. Individual beads submerged in saline were compressed at a constant strain rate (~1-2%/s) generating a force displacement curve that was analyzed with Hertzian contact mechanics for the linear elastic deformation of a sphere compressed between two surfaces according to the equation below (N=20).

$$E^* = \frac{3 F}{4 h^{3/2} \sqrt{R^*}}$$

where  $E^*$  is the indentation modulus,  $E / (1-\nu^2)$  where  $E$  is Young's modulus and  $\nu$  is Poisson's ratio.  $F$  is the force,  $h$  is the displacement and  $R^*$  is the relative curvature between the sphere and the surface.

#### Bead Suspension, Catheter Deliverability and Iodine Concentration Selection

A durable bead suspension is desirable for ease of delivery during an embolization procedure. Beads

that rapidly settle are not channeled into the catheter at a uniform rate leading to unpredictable delivery. RO beads suspension lifetimes and delivery properties were evaluated in a syringe-based model to mimic clinical practice. A range of bead sizes and non-ionic contrast agents including iohexol (Omnipaque 350, GE Healthcare), iodixanol (Visipaque 270 and 320, GE), iomeprol (Iomeron 300 and 400, Bracco) and iopamidol (Isovue 300, Bracco) were evaluated. A sample of RO beads was removed from a vial through an 18 G needle with a 10 mL syringe. The beads were allowed to settle in the syringe and the packing solution was expelled until a slurry of beads remained. With a 20 mL syringe, contrast agent (a multiple of 10 times the volume of beads) was mixed with the bead slurry through a 3-way connector. The 20 mL syringe was removed and replaced with a 3 mL syringe. The solution was mixed between the 3 mL and 10 mL syringe until a homogenous suspension was achieved, the 3 mL syringe was held horizontally in place against a dark background and the suspension durability was timed by monitoring the sedimentation of the beads to 70% of the horizontal barrel height (N=3). Further experiments were performed on the impact of saline to contrast ratio (contrast:saline = 100:0, 90:10, 80:20, 70:30, 60:40 and 50:50, N=10) and the influence of bead size. Catheter deliverability was determined by administering a homogenous bead suspension in 100% iohexol (1:10 bead dilution, 1 or 3 mL syringe). The catheters were laid on a bench, and at the center of the catheter a coil (10 cm diameter) was introduced to produce a more tortuous path for the beads to navigate around, and representing the curvature catheters may experience in a patient. Any catheter clogging was recorded as a failure and denoted that bead size was not suitable to the respective catheter. Catheters included 1.9-Fr Prowler Select LP ES (Codman, Raynham, MA), 2.3-Fr Prowler Select Plus (Codman), 2.4-Fr and 2.8-Fr Progreat (Terumo, Somerset, NJ), and 4.0-Fr Radiofocus glidecath (Terumo).

In pilot studies, a series of RO Beads with varying degrees of iodination were evaluated during independent sessions by 4 blinded interventional radiologists experienced in embolotherapy. RO Beads syringe handling and catheter deliverability were assessed. A level of iodination was selected that provided the best balance between the ability to handle and administer the beads with the highest acceptable level of iodination (for increased X-ray visibility). The optimum performance was achieved with iodine concentration of ~150 mg iodine/mL sedimented bead volume. RO Beads were also evaluated in pilot animal studies to assess the *in vivo* radiopacity. These pilot studies formed the basis for the iodine concentration selection used herein.

### *In Vitro* Penetration

A schematic of the experimental set-up of an apparatus to measure bead penetration properties is shown in supplemental information (Figure S1). A Delrin base was machined to create a central region with a gap gradient which ranges from 555  $\mu\text{m}$  at one end (entrance) to 25  $\mu\text{m}$  at the other end (exit of the plate) over a 200 mm length. A glass plate to enable visualization was positioned over the gradient and clamped into position, creating a triangular wedge-shaped interior volume. The three sides of the glass plate were sealed by a nitrile rubber seal which was recessed into the Delrin, the end of the plate at the thin end of the gradient was left open to allow the carrier fluid (0.9% saline solution) to freely exit. The beads carrier fluid entered the device at the wide end of the gradient. The carrier fluid was held in a reservoir raised 54.4 cm above the penetration device resulting in a pressure of 40 mmHg to emulate circulatory blood pressure in appropriately sized vessels. A bead slurry of 0.5 mL of sedimented beads was introduced via an injection port into the carrier fluid line, whereby the fluid flow carried the beads into the penetration device until they were physically constrained by their size and could not migrate further into the narrowing gap. This was performed for the following LC Bead and RO Beads size ranges: 40-90, 70-150, 100-300 and 300-500  $\mu\text{m}$ . A picture of the beads within the plate assembly was captured using a digital camera and the maximum and minimum penetration where measured (N=3).

### Radiopaque Beads Phantom Preparation

A 1% agarose solution was prepared by mixing agarose powder (0.2 g, Sigma Aldrich, Poole UK) with deionized water (20 mL) at room temperature and heating to 90°C with constant stirring. Once all the agarose had dissolved, the temperature was reduced to 42°C. RO Beads were suspended in deionized water and progressively diluted to produce series of desired concentrations. Each dilution was mixed with an equal volume of agarose and a static uniform bead-agarose suspension was prepared by repeatedly withdrawing and expelling the solution using a manual pipette. This gelatinous suspension is generally referred to as a homogeneous phantom [14]. Line phantoms were similarly prepared except tubes of known inner diameters (0.28, 0.40, 0.58, 0.86 and 1.02 mm) were first filled with beads in deionized water prior to setting the filled tubes in an agarose matrix.

### *In Vitro* Micro-Computed Tomography

Homogeneous bead phantoms were analyzed with micro-CT (Reading Scientific Services Ltd, Reading, UK) using a Bruker SkyScan 1172 micro-CT

scanner (Kontich, Belgium). Each bead phantom was imaged at 64 kVp, 155  $\mu\text{A}$  and an aluminum filter (500  $\mu\text{m}$ ). The samples were then reconstructed using NRecon and calibrated against a volume of interest of air and purified water to yield Hounsfield Units (HU) for individual RO Bead (N=10).

### *In Vitro* 2D X-ray

RO Beads line phantoms were imaged using a Philips Allura Xper FD20 system (7.6.3, Philips Healthcare, Best, The Netherlands), using clinically available settings for fluoroscopy (75 kVp, 133 mA, 7 ms, 15 frames/s, and 0.1 mm Cu filter) and X-ray single shot (80 kVp, 529 mA, 65 ms) with standard Allura Xper image processing. Only contrast and brightness settings were adjusted to enhance visibility. Measurements to model patient absorption (21.6 cm of PMMA) with a 42 cm detector format at a 110 cm source to image-receptor distance were performed by positioning the line phantoms on PMMA slabs. Images were read by two board-certified interventional radiologists with 3 and 9 years of experience to determine whether the lines were detectable.

### *In Vitro* Multidetector Computed Tomography

Homogenous bead phantoms (5 series of 6 serially diluted phantoms) were imaged using a 320-detector-row MDCT scanner (Aquillon One, Toshiba, Japan). A six factor serial dilution of RO Beads was prepared ranging from 12.5 to 0.39% sedimented bead volume. Imaging parameters were: 120 kVp, 350 mA, 0.5 mm collimator with 3D reconstruction resulting in 0.5 mm slice thickness and field of view (FOV) of 22x22 cm.

### *In Vivo* Experiments

#### Animal Tumor Model

Adult female New Zealand white rabbits (Millbrook Breeding Labs, Amherst, MA) weighing 4.1-5.1 kg were used in accordance with institutional guidelines under an approved animal care and use committee protocol. Food and water was allowed *ad libitum*. VX2 tumor chunks from previous experiments were injected into the hind legs of carrier rabbits, where the tumor was grown for 2 weeks. Each carrier was used to supply recipients for tumor implantation into the liver. Each recipient animal received tumor implantation in the left lobe of the liver as detailed in previous publication [25]. The tumors were allowed to grow in the livers for 2 weeks, after which time a well demarcated solitary tumor was expected to grow to a size of about 2.0 cm in diameter [26].

### **In Vivo Experimental Design**

Animals were randomized into 3 hepatic intra-arterial treatment groups and received an infusion of either: (a) LC Bead + soluble contrast medium (iodixanol, 320 mgI/ml) (n=5), (b) RO Beads + soluble contrast medium (iodixanol, 320 mgI/ml) (n=6) and (c) RO Beads + dextrose (Dextrose in water 50%, Hospira inc., Lake Forest, IL) (n=4). RO Beads in dextrose was used to evaluate the conspicuity of RO Beads alone to overcome the confounding contribution of iodine in the soluble contrast medium for X-ray visibility. Dextrose was chosen as a radiolucent suspension medium providing higher viscosity and density (specific gravity: 1.17) than saline, allowing for a better suspension. LC Bead and RO Beads were supplied in sealed glass vials in the size range of 70-150  $\mu\text{m}$ . A bead suspension was withdrawn into a syringe and any excess solution was expelled. The segmented bead volume was measured in the syringe and then diluted 1:20 in the appropriate suspension medium.

### **Transarterial Embolization**

The procedure was performed as previously reported [25, 26]. Briefly, surgical cut down was done on pre-anesthetized rabbits (isoflurane 1.5-3%) to gain access into the common femoral artery followed by the placement of a 3-Fr vascular sheath (Cook, Inc., Bloomington, IN). A 2.1/1.7-Fr microcatheter (Echelon 10, ev3 Endovascular, Inc., Plymouth, MN) was manipulated into the celiac axis, after which a celiac arteriogram was performed to delineate the blood supply to the liver. The proper hepatic artery was then selectively catheterized; this was occasionally performed with the aid of a steerable guide wire (0.014 in. Transcend wire; Boston Scientific Oncology, Natick, MA). The tumor was visualized on digital subtraction angiography (DSA) as a region of hypervascular blush located in the left liver lobe. The embolization was performed from the proper hepatic artery, instead of a more distal and selective position, to ensure sufficient forward flow in a larger blood vessel to better mimic delivery in a clinical setting. The various treatment regimens (delivered in 0.05 mL aliquots of sedimented bead volume) were administered under real-time fluoroscopy. Upon completion of the treatment and imaging, animals were sacrificed.

### **In Vivo Imaging**

Intraprocedural imaging was performed using a C-arm system (Allura Xper FD20, Philips Healthcare, Best, The Netherlands) with the XperCT option enabling C-arm CBCT. Each animal underwent a DSA to identify the tumor location and appearance. Once contrast washout was confirmed on all imaging mo-

dalities (>30 min from DSA), fluoroscopy, X-ray single shot and CBCT images were acquired to document baseline appearance, followed by treatment delivery in a series of aliquots with interval imaging. A fluoroscopy loop and X-ray single shot were acquired following administration of each aliquot. CBCT was obtained after administration of 0.1 cc of sedimented bead volume and at the end of the procedure. Additional CBCT and high dose CBCT images were obtained following euthanasia, where cardiorespiratory motion artifacts were no longer factors affecting image quality.

Imaging modalities included live fluoroscopy (15 frames/sec; 85 kV; 23 mA; 45 ms; binning 2x2), X-ray single shot (70 kV; 23 mA; 45 ms; binning 1x1; pixel: 0.154x0.154 mm), CBCT (low dose - 30 frames/sec; 10 sec scan; 312 images; 80 kVp; 325 mA; 3 ms; resolution: 0.98x0.98x0.98 mm<sup>3</sup>; FOV: 25x25x19 cm; matrix size: 256x256x198); high dose CBCT (30 frames/sec; 20 sec scan; 624 images; 80 kVp; 650 mA; 3 ms; resolution: 0.98x0.98x0.98 mm<sup>3</sup>; FOV: 25x25x19 cm; matrix size: 256x256x198).

### **Image Analysis**

Qualitative image description was performed in consensus by two board-certified interventional radiologists (3 and 9 years of experience) who participated in the procedures. Semi-quantitative image analysis was performed in independent reading sessions by 6 board-certified interventional radiologists who did not participate in the embolization procedures. The scoring system was comprised of 2 features to assess visibility: 1) contrast visibility in target arteries (5-point scale - very good, good, barely acceptable, poor and very poor) and 2) contrast visibility in non-target arteries (5-point scale). Representative images were chosen from fluoroscopy loops during injection (2 examples), single fluoroscopy after delivery, X-ray single shot after aliquot delivery (2 examples) and post-euthanasia high-dose CBCT. The reading scores were averaged between observers and reported per imaging modality within each group. Imaging analysis was performed using DICOM viewer software (OsiriX MD version 6.0.1, Switzerland).

### **Statistical Analysis**

Experiment data were expressed as mean  $\pm$  standard deviation (SD). The bead diameter, minimum, maximum, range, average, SD and frequency distribution were calculated. For each reader, the responses were ranked across all rabbits. The averages of these ranks across the readers for each rabbit were analyzed using Wilcoxon two-sample tests to perform pairwise comparisons between the treatment groups.

Statistical significance was defined as a 2-sided *P*-value <0.05. Statistical analysis was performed using Prism 6 (GraphPad Software, Inc., La Jolla, CA) and SAS (SAS Institute, 9.2., Cary, NC).

## Results

### Bench-top Experiments

#### Bead Physical Property Characterization

RO Bead was synthesized by replacing the blue dye with a triiodobenzyl moiety that imparts the benefit of both a visible yellow tint and a high degree of radiopacity. Similar to LC Bead, the RO Beads were highly spherical and smooth (Figure 2A-D). RO Beads were sieved into 4 calibrated size ranges resulting in narrow size distributions (Figure 2E and Table 1) that conformed well to the labeled size range like that found in LC Bead with a coefficient of variance from 11 - 34%.

**Table 1:** RO Bead size properties (N = 200-214).

Size(μm)	Mean diameter ± SD (μm)	Range (min - max) (μm)
40-90	68 ± 8.7	44 - 85
70-150	98 ± 12.6	75 -132
100-300	164 ± 55.2	78 - 327
300-500	361 ± 40.8	300 - 489

LC Bead has high EWC (96%) and a density of ~1.05 g/cc [27]. In comparison, the covalent attachment of triiodobenzyl moieties to RO Beads confers a

more hydrophobic and dense bead structure, resulting in a density of 1.21-1.36 g/cc, EWC of 60-72% and ~100-fold greater elastic compression modulus than LC Bead (Table 2, Table S1). The RO Beads synthetic route provided a great degree of flexibility and control over the degree of bead iodination (~25-250 mg iodine/mL sedimented beads). The iodine concentration of RO Beads (~150 mg iodine/mL sedimented beads) used herein was chosen to balance radiopacity with handling performance. This was found to be where the iodine concentration within the bead approached the concentration of commonly used soluble iodinated contrast medium (range = ~190-260 mg iodine/mL true bead volume; Table 2).

#### Handling and Delivery Performance

The density and viscosity of the soluble iodinated contrast media influenced the suspension lifetime. Iodixanol 320 and iomeprol 400 produced durable suspensions of 9 min and 50 min, respectively. Other soluble contrast media produced suspensions in the range of 30 sec to 4 min. Any dilution of soluble contrast media with saline greatly reduced the suspension lifetime (e.g., 9 min, 6 min and 1.5 min for 100%, 90% and 80% iodixanol 320, respectively). Suspension duration was also inversely proportional to bead size. Suspension lifetimes for various soluble iodinated contrast media type and bead size may be found in Table S2 and S3.

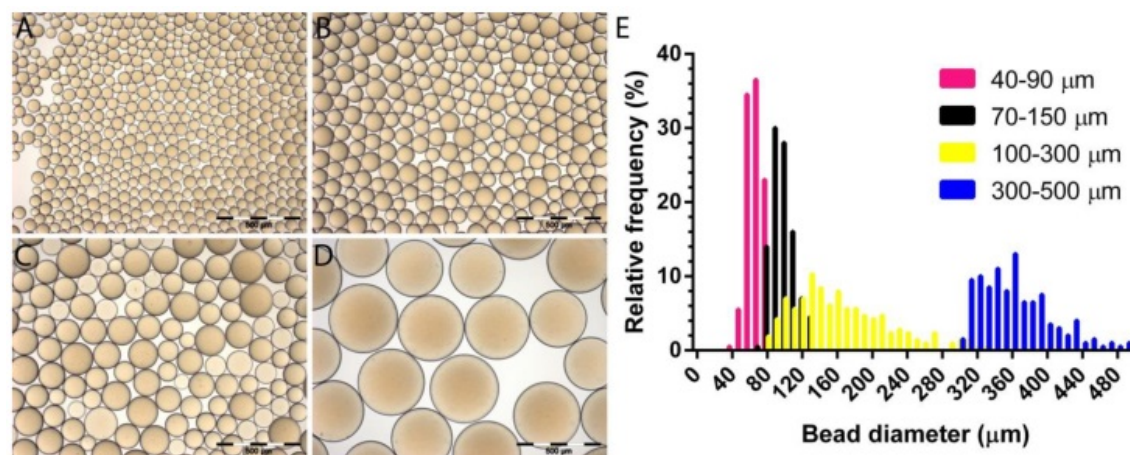


**Figure 2:** Optical micrographs of RO Beads. A) 40-90 μm, B) 70-150 μm, C) 100-300 μm and D) 300-500 μm. E) Relative frequency distribution of RO Beads size measured with an optical microscope (N = 200-214).

**Table 2:** Physical properties of RO Beads.

Size(μm)	Mean density ± SD (g/mL)	EWC (%)	Elastic modulus ± SD (MPa)	Iodine concentration (mg iodine/mL sedimented beads)	Iodine concentration (mg iodine/mL true bead volume)
40-90	1.36 ± 0.112	66.6	30.0 ± 3.01	150.1	245.5
70-150	1.31 ± 0.075	60.1	39.4 ± 10.19	176.9	258.4
100-300	1.26 ± 0.090	66.6	27.2 ± 5.46	155.0	229.4
300-500	1.21 ± 0.025	71.9	11.2 ± 0.42	132.5	188.9

Catheter deliverability was investigated in a range of common catheters as shown in Table 3. 40-90 and 70-150  $\mu\text{m}$  RO Beads were successfully delivered through all catheters investigated down to 1.9-Fr. 100-300 and 300-500  $\mu\text{m}$  RO Beads passed catheters as small as to 2.3-Fr and 4-Fr, respectively.

**Table 3:** Catheter deliverability of various size RO Beads.

RO Beads Size ( $\mu\text{m}$ )	1.9-Fr (ID = 419 $\mu\text{m}$ )	2.3-Fr (ID = 533 $\mu\text{m}$ )	2.4-Fr (ID = 559 $\mu\text{m}$ )	2.8-Fr (ID = 686 $\mu\text{m}$ )	4-Fr (ID = 1,003 $\mu\text{m}$ )
40-90	Pass*	Pass	Pass	Pass	Pass
70-150	Pass*	Pass	Pass	Pass	Pass
100-300	Fail	Pass	Pass	Pass	Pass
300-500	Fail	Fail	Fail	Fail	Pass

\*40-90  $\mu\text{m}$  and 70-150  $\mu\text{m}$  delivered using a 1 mL syringe with a 1.9-Fr only. 3 mL syringe used for larger catheters. ID: inner diameter.

### In Vitro Penetration

LC Bead and RO Beads penetrated to similar levels within the specified size range (Figure 3). Importantly, selection of a bead size range provided precise control over the level of embolization.

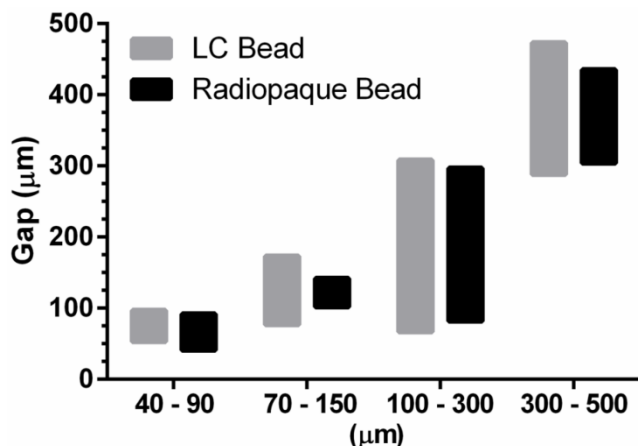


**Figure 3:** *In vitro* penetration assay for LC Bead and Radiopaque Bead. The bar graphs depict penetration potential according to bead size. The bottom of the bar is the maximum penetration of the bead and the top of the bar is the trailing edge of a bead population (0.5 mL aliquot of sedimented beads). The maximum penetration and the trailing edge for each size range was measured and displayed as an average (N=3).

### In Vitro Radiopacity

RO Beads were evaluated with micro-CT to determine their radiopacity and distribution of iodine within the bead as shown in Figure 4. A homogeneous RO Beads (100-300  $\mu\text{m}$ ) phantom is shown as a single 2D projection in Figure 4A and as a single slice through a reconstructed 3D dataset in Figure 4B. These images demonstrate similar attenuation of each bead, suggesting that the iodination was uniform

throughout the bead population. Moreover, examination of individual bead cross-sections (Figure 4C) revealed a uniform distribution of iodine throughout the bead interior (confirmed by energy dispersive X-ray spectroscopy on bead sections, data not shown). The average attenuation of each RO Bead was  $5639 \pm 228.8$  HU (158 mg iodine/mL sedimented beads).

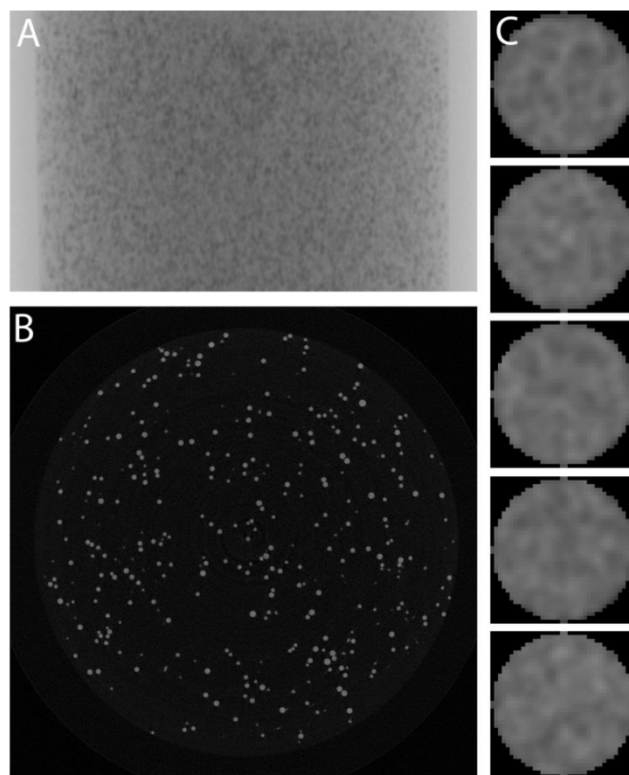


**Figure 4:** Micro-CT of homogeneous RO Beads phantoms. A) Single 2D projection, B) Slice through reconstructed data, and C) Column of individual beads (~160  $\mu\text{m}$  diameter).

RO Beads line phantoms were imaged with typical clinical parameters to determine the idealized (lack of cardiorespiratory motion) minimum diameter blood vessel that may be detected (Figure 5A). The image quality of X-ray single shot was greater than standard fluoroscopy due to the greater X-ray flux and non-binning. The 0.86 mm diameter lines were detectable using fluoroscopy and X-ray single shot allowed detection of lines as narrow as 0.4 mm. Increasing attenuation was measured on MDCT with decreasing serial dilution, reaching an average attenuation of  $365.46 \pm 47.26$  HU (12.5% sedimented bead volume) compared to  $21.17 \pm 9.82$  HU (0.39% sedimented bead volume).

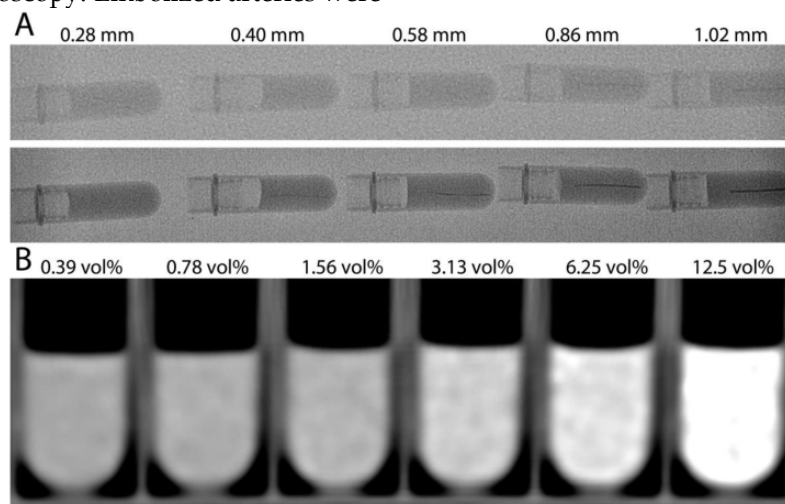
### In Vivo Performance

Figure 6 illustrates a representative animal of each group. The soluble contrast medium was sufficient to identify target and non-target embolization on

real-time fluoroscopy during administration, independent of bead type. When soluble contrast medium was omitted, RO beads alone were not sufficient to visualize embolization (Figure 6, RO Beads + dextrose, top row). However when the blood flow was slow towards the end of the embolization process, RO beads were faintly visible in transit on real-time fluoroscopy. Imaging appearance with fluoroscopy diminished over time for LC Bead as soluble contrast medium “washed out” of the blood vessels. Importantly, RO Beads demonstrated more persistent conspicuity on fluoroscopy. X-ray single shot demonstrated better imaging appearance of RO Beads versus LC Bead, most likely due to the washout of contrast in the LC Bead group and better image quality of X-ray single shot than fluoroscopy. Embolized arteries were

better evidenced with progressive embolization of RO Beads compared to LC Bead on X-ray single shot.

Following the embolization procedure with RO Beads suspended in soluble contrast medium and euthanasia, high dose CBCT demonstrated contrast retention in the tumor (Figure 7, short arrows) and opacification of hepatic arteries (Figure 7, arrow heads). Furthermore, non-target embolization of extrahepatic arteries (Figure 7, long arrow) was clearly observed. In general, RO Beads in soluble contrast medium had improved imaging appearance in target and non-target blood vessels compared to LC Bead delivered in soluble contrast medium. RO Beads conspicuity was durable *in vivo*, lasting to at least 7 days (data not shown).



**Figure 5:** A) 2D X-ray images of RO Beads line phantoms. Standard fluoroscopy (top row) and X-ray single shot (bottom row) show a series of microfuge tubes with horizontal line phantoms mimicking blood vessels of various inner diameters. B) Multidetector computed tomography of RO Beads phantoms with a six factor serial dilution of RO Beads ranging from 12.5 to 0.39% sedimented bead volume (vol%).

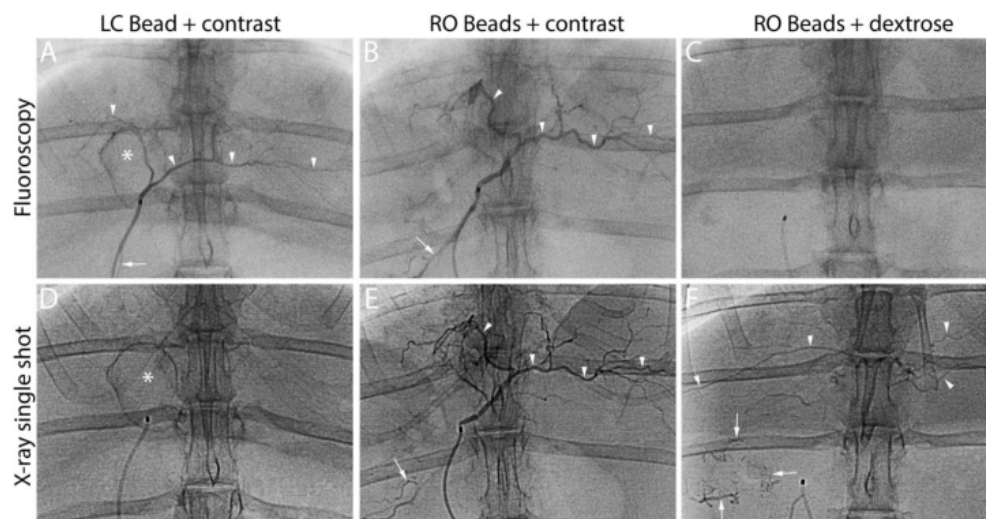


**Figure 6:** LC Bead in iodinated soluble contrast medium (LC Bead+contrast), RO Beads in iodinated soluble contrast medium (RO Beads+contrast) and RO Beads in dextrose (RO Beads+dextrose) on real-time fluoroscopy during administration and X-ray single shot following delivery. Arrowheads indicate target artery opacification whereas arrows highlight reflux into non-target arteries. \*Identifies the gallbladder.

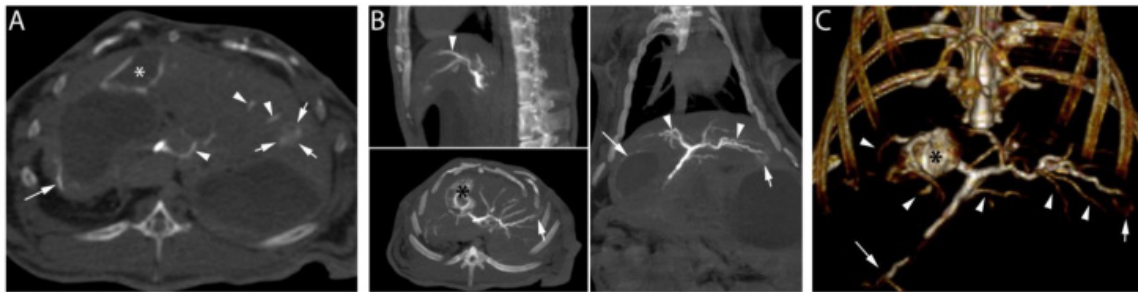


**Figure 7:** High dose CBCT performed post-euthanasia after the delivery of 1.1 cc of RO Beads suspension (0.055 cc RO Beads sedimented volume) delivered in iodinated soluble contrast medium. A) Axial image: contrast retention in the tumor is observed (short arrows). Linear attenuation in the wall of the gallbladder (asterisk) and hepatic arteries (arrowheads) are evidenced. Non-target delivery is shown in a gastric artery in the wall of the stomach (long arrow). B) Multi-planar reconstruction demonstrated contrast retention in the tumor located in the left hepatic lobe (short arrows). Linear attenuation consistent with a tumor feeding and normal hepatic arteries is also shown (arrowheads). Contrast retention is observed in the wall of the gallbladder (black asterisk). Non-target delivery is shown in gastric arteries and the wall of the stomach (long arrow). C) 3D volume rendering image in coronal view demonstrating the hepatic arteries (arrowheads), non-target delivery (long arrow), the tumor located in the left hepatic lobe (short arrow) and hyperattenuation of the wall of the gallbladder (black asterisk).

An objective reading study was performed to assess the conspicuity of RO Beads and potential benefit over LC Bead as shown in Figures 6 and 7. Soluble contrast medium improved the visibility in target and non-target arteries during delivery on real-time fluoroscopy (LC Bead + contrast vs. RO Beads + dextrose,  $P=0.0079$ ,  $P=0.0159$ ; RO Beads + contrast vs. RO Beads + dextrose,  $P=0.0048$ ,  $P=0.0095$  [target and non-target, respectively]). After injection of a bead aliquot, RO Beads were similar to LC Bead in terms of visibility on fluoroscopy (LC Bead + contrast vs. RO Beads + contrast,  $P=0.0886$ ,  $P=0.2468$  [target and non-target, respectively]). However, immediately after injection of a bead aliquot, RO Beads + contrast significantly increased visibility on X-ray single shot compared to LC Bead + contrast ( $P=0.0043$  and  $P=0.0043$  in target and non-target arteries, respectively). Similarly, RO beads significantly improved visibility over LC Bead on CBCT in target arteries ( $P=0.0238$ ) and showed a clear trend towards better visibility in non-target arteries ( $P=0.0519$ ).

## Discussion

The main finding of our study is that RO Beads provided better conspicuity to determine target (visualized using X-ray single shot and CBCT) and non-target (visualized using X-ray single shot) embolization as compared to LC Bead while optimally balancing the handling and delivery performance with the requirement for a high degree of radiopacity. This finding may constitute a major technical improvement for embolotherapy to treat liver cancer compared to currently available radiolucent LC Bead.

Embolotherapy with radiolucent beads relies on indirect signs compared to conventional Lipiodol-based TACE, in which the treatment delivery is readily visible due to the inherent radiopacity of the drug delivery vehicle itself (the iodinated poppy-seed

oil) [2, 28]. Indeed, the exact distribution of radiolucent beads currently used to treat liver tumors is unknown and the assessment of treatment is based on the visualization of retained soluble contrast in the target tissue area and/or lack of contrast enhancement after treatment of previously enhancing lesions [3-6]. These intra-procedural image-based signs are temporary and vanish quickly as soluble contrast medium washes out. Hence, it is crucial to improve image-based feedback in real-time during the course of the embolization to improve treatment precision and provide the best opportunity for the operator to personalize the treatment for a specific patient.

To prepare an optimal RO Bead, it is desirable to have a process that allows precise control over the degree of radiopacity imparted to the bead. Starting with PVA as a base hydrogel material was useful in this aspect as it has multiple hydroxyl groups that could be utilized for chemical attachment of the radiopaque moieties into the bead structure. RO Bead was produced using a one-step coupling reaction to attach triiodobenzyl groups to preformed beads. This method imparted a yellow coloration, instead of blue for LC Bead, and importantly conferred radiopacity under X-ray based imaging. The resulting individual RO Bead demonstrated a uniform iodine distribution throughout their interior structure and a consistent radiopacity across a bead population, indicating that the reaction was particularly efficient despite being conducted on a preformed hydrogel matrix. The triiodobenzyl unit was chosen because it is the basis for many contrast agents as it provides a high content of iodine per unit mass. Preliminary studies that evaluated the balance of handling and delivery performance established the optimum iodine concentration of  $\sim 150$  mg iodine/mL sedimented bead volume. Interestingly, this corresponds to  $\sim 250$  mg/mL of true bead volume, which is comparable to the concentra-

tion of iodine in commonly used soluble iodinated contrast agents.

The manufacturing process for RO Beads yielded equivalent size ranges to LC Bead. In addition to LC Bead, a smaller 40-90  $\mu\text{m}$  size range of RO Beads was produced. Similar to LC Bead, RO Beads were spherical and smooth hydrogels. However, the incorporation of a hydrophobic radiopaque species increased their density ( $\sim 1.3 \text{ g/cc}$  versus  $\sim 1 \text{ g/cc}$ ) and decreased their EWC ( $\sim 65\%$  versus  $\sim 95\%$ ). This increased density resulted in a shorter suspension lifetime compared to LC bead. However, use of 100% iodixanol rather than dilute contrast resulted in a clinically practical and durable suspension, comparable to LC Bead. This durable bead suspension is desirable for ease of delivery during an embolization procedure as beads that rapidly settle in the delivery syringe are not channeled into the catheter at a uniform rate, leading to unpredictable and problematic delivery including proximal occlusion [29].

Microspherical embolic agents composed of deformable hydrogels are often designed to temporarily deform in a catheter and re-expand upon release into the artery in order to aid in delivery when the inner diameter of the catheter is smaller than the bead diameter [27]. The lower EWC of RO Beads inferred a more collapsed hydrogel network leading to a  $\sim 100$ -fold greater elastic compression modulus than LC Bead. This greater stiffness of RO Beads affected its deliverability compared to LC Bead. Despite this limitation, RO Beads  $\leq 300 \mu\text{m}$  were still able to be delivered through a 2.3-Fr microcatheter, which is acceptable for the majority of embolotherapy procedures. Furthermore, *in vitro* testing showed that RO beads penetrated to the same maximum extent as LC Bead.

RO Beads had similar X-ray visibility compared to LC Bead when soluble contrast medium was used during real-time treatment delivery (i.e. live fluoroscopy). As expected, soluble contrast medium was sufficient to visualize target and non-target embolization during delivery. However, the presence of RO Beads clearly demonstrated increased image contrast visibility in target tissues on immediate and on interval post-injection imaging with X-ray single shot and CBCT compared to LC Bead. Importantly, the presence of RO Beads also helped to identify non-target delivery. Moreover, with progressive embolization, the durable radiopacity of RO Beads aided in the evaluation of completeness of the planned embolization. These findings highlight the limitation of rapid soluble contrast washout over time. Clinically, these observations may lead to intra-procedural changes in treatment planning and help to guide post-procedure patient management accordingly. Indeed, the im-

proved visualization of RO Beads over LC Bead described herein suggests that RO Beads may provide additional intra-procedural clinical benefit by (i) enabling the identification of tumor regions at risk of being under-treated; (ii) allowing the identification of non-target embolization to modify the procedure in real-time and (iii) contributing towards embolization end-point determination. Furthermore, post-procedural clinical benefit may be obtained by (i) optimizing post-procedure patient care (e.g. identification of non-target embolization) and (ii) marking the embolized vessels for subsequent therapy (e.g., additional embolization or combined treatment with radiofrequency or microwave ablation).

There were several limitations in our study. First, *in vivo* radiopacity was evaluated in rabbits that have less attenuation than human patients. Thus real-life RO Beads performance will not be known until first-in-human studies are performed. Furthermore, image quality degradation due to the higher frequency of cardiorespiratory motion in rabbits is more problematic than in patients. Second, pathological analysis of the RO Beads effect on tissues was not evaluated and both target and non-target embolization was not validated histologically; further experimental studies are needed. Yet our study focused on the periprocedural assessment of RO Beads to reflect clinical practice.

In conclusion, RO Beads described in our study may provide a practical and improved alternative to currently used microspherical embolization agents by offering better conspicuity to determine target and non-target embolization. Furthermore, the durable imaging appearance of RO Beads may also aid in the guidance and evaluation of the embolization procedure.

## Supplementary Material

Figure S1, Tables S1- S3.

<http://www.thno.org/v06p0028s1.pdf>

## Abbreviations

TAE: transarterial embolization; TACE: transarterial chemoembolization; PMMA: poly(methylmethacrylate); PVA-AMPS: acrylamido polyvinyl alcohol-co-acrylamido-2-methylpropane sulfonate; EWC: equilibrium water content; MDCT: multidetector computed tomography; CBCT: cone beam computed tomography; RO: radiopaque; HU: Hounsfield Units; DSA: digital subtraction angiography; FOV: field of view.

## Acknowledgements

We thank Dr. Samuel Greene, Dr. Brian P. Holly, Dr. John D. Werner and Dr. A. Tamrazi for their con-

tribution to reading study. We thank Dr. Nikhil Chauhan for statistics and Dr. Andy Bushby for mechanical testing.

## Competing Interests

**Financial Support:** Our study was funded by NIH/NCI R01 CA160771 and by Biocompatibles UK Ltd, a BTG International group company.

**Disclosures:** Jean-François H. Geschwind, M.D.: Consultant: Biocompatibles/BTG, Bayer HealthCare, Guerbet, Nordion/BTG, Philips Healthcare and Jennerex. Grant Support: Biocompatibles/BTG, Bayer HealthCare, Philips Healthcare, Nordion/BTG, Threshold, Guerbet, DOD, NCI-ECOG and NIH-R01. Founder and CEO PreScience Labs, LLC. Koorosh Ashrafi, Matthew R. Dreher, Andrew L. Lewis and Sean Willis are paid employees of Biocompatibles UK Ltd, a BTG International group company. MingDe Lin, Alessandro Radaelli and Mark den Hartog are Philips Employees. Karun Sharma is a consultant to Biocompatibles/BTG.

## References

- Avritscher R, Wallace MJ. Chapter 7: Principles of Embolization. New York: Springer; 2011.
- Lewandowski RJ, Geschwind JF, Liapi E, Salem R. Transcatheter intraarterial therapies: rationale and overview. *Radiology*. 2011; 259: 641-57.
- Golowa YS, Cynamon J, Reinus JF, Kinkhabwala M, Abrams M, Jagust M, et al. Value of noncontrast CT immediately after transarterial chemoembolization of hepatocellular carcinoma with drug-eluting beads. *J Vasc Interv Radiol*. 2012; 23: 1031-5.
- Loffroy R, Lin M, Yenokyan G, Rao PP, Bhagat N, Noordhoek N, et al. Intra-procedural C-arm dual-phase cone-beam CT: can it be used to predict short-term response to TACE with drug-eluting beads in patients with hepatocellular carcinoma? *Radiology*. 2013; 266: 636-48.
- Wang X, Erinjeri JP, Jia X, Gonen M, Brown KT, Sofocleous CT, et al. Pattern of retained contrast on immediate postprocedure computed tomography (CT) after particle embolization of liver tumors predicts subsequent treatment response. *Cardiovasc Intervent Radiol*. 2013; 36: 1030-8.
- Suk Oh J, Jong Chun H, Gil Choi B, Giu Lee H. Transarterial chemoembolization with drug-eluting beads in hepatocellular carcinoma: usefulness of contrast saturation features on cone-beam computed tomography imaging for predicting short-term tumor response. *J Vasc Interv Radiol*. 2013; 24: 483-9.
- Horak D, Metalova M, Svec F, Drobnik J, Kalal J, Borovicka M, et al. Hydrogels in endovascular embolization. III. Radiopaque spherical particles, their preparation and properties. *Biomaterials*. 1987; 8: 142-5.
- Thanoo BC, Jayakrishnan A. Radiopaque hydrogel microspheres. *J Microencapsul*. 1989; 6: 233-44.
- Thanoo BC, Jayakrishnan A. Barium sulphate-loaded p(HEMA) microspheres as artificial emboli: preparation and properties. *Biomaterials*. 1990; 11: 477-81.
- Thanoo BC, Jayakrishnan A. Tantalum loaded silicone microspheres as particulate emboli. *J Microencapsul*. 1991; 8: 95-101.
- Thanoo BC, Sunny MC, Jayakrishnan A. Preparation and properties of barium sulphate and methyl iothalamate loaded Poly(vinyl alcohol) microspheres as radiopaque particulate emboli. *Journal of Applied Biomaterials*. 1991; 2: 67-72.
- Mawad D, Poole-Warren LA, Martens P, Koole LH, Slots TL, van Hooy-Corstjens CS. Synthesis and characterization of radiopaque iodine-containing degradable PVA hydrogels. *Biomacromolecules*. 2008; 9: 263-8.
- Saralidze K, van Hooy-Corstjens CS, Koole LH, Knetsch ML. New acrylic microspheres for arterial embolization: combining radiopacity for precise localization with immobilized thrombin to trigger local blood coagulation. *Biomaterials*. 2007; 28: 2457-64.
- Sharma KV, Dreher MR, Tang Y, Pritchard W, Chiesa OA, Karanian J, et al. Development of "imageable" beads for transcatheter embolotherapy. *J Vasc Interv Radiol*. 2010; 21: 865-76.
- van Hooy-Corstjens CS, Saralidze K, Knetsch ML, Emans PJ, de Haan MW, Magusin PC, et al. New intrinsically radiopaque hydrophilic microspheres for embolization: synthesis and characterization. *Biomacromolecules*. 2008; 9: 84-90.
- Hasan MS, Kehoe S, Boyd D. Temporal analysis of dissolution by-products and genotoxic potential of spherical zinc-silicate bioglass: "imageable beads" for transarterial embolization. *J Biomater Appl*. 2014; 29: 566-81.
- Cilliers R, Song Y, Kohlmeier EK, Larson AC, Omary RA, Meade TJ. Modification of embolic-PVA particles with MR contrast agents. *Magn Reson Med*. 2008; 59: 898-902.
- Gupta T, Virmani S, Neidt TM, Szolc-Kowalska B, Sato KT, Ryu RK, et al. MR tracking of iron-labeled glass radioembolization microspheres during transcatheter delivery to rabbit VX2 liver tumors: feasibility study. *Radiology*. 2008; 249: 845-54.
- Lee KH, Liapi E, Vossen JA, Buijs M, Ventura VP, Georgiades C, et al. Distribution of iron oxide-containing Embosphere particles after transcatheter arterial embolization in an animal model of liver cancer: Evaluation with MR Imaging and implication for therapy. *J Vasc Interv Radiol*. 2008; 19: 1490-6.
- Namur J, Chapot R, Pelage JP, Wassef M, Langevin F, Labarre D, et al. MR imaging detection of superparamagnetic iron oxide loaded tris-acryl embolization microspheres. *J Vasc Interv Radiol*. 2007; 18: 1287-95.
- Seevinck PR, Seppenwoolde JH, Zwanenburg JJ, Nijssen JF, Bakker CJ. FID sampling superior to spin-echo sampling for T2\*-based quantification of holmium-loaded microspheres: theory and experiment. *Magn Reson Med*. 2008; 60: 1466-76.
- Bartling SH, Budjan J, Aviv H, Haneder S, Kraenzlin B, Michaely H, et al. First multimodal embolization particles visible on x-ray/computed tomography and magnetic resonance imaging. *Invest Radiol*. 2011; 46: 178-86.
- Oerlemans C, Seevinck PR, Smits ML, Hennink WE, Bakker CJ, van den Bosch MA, et al. Holmium-lipiodol-alginate microspheres for fluoroscopy-guided embolotherapy and multimodality imaging. *Int J Pharm*. 2015; 482: 47-53.
- Lewis AL, Heasysman CL. Biomedical Applications of Hydrogels: Poly(vinyl alcohol)-Based Hydrogels for Embolotherapy and Drug Delivery. In: *Polymeric and Self Assembled Hydrogels: From Fundamental Understanding to Applications*. Royal Society of Chemistry; 2012: 232-252.
- Hong K, Khwaja A, Liapi E, Torbenson MS, Georgiades CS, Geschwind JF. New intra-arterial drug delivery system for the treatment of liver cancer: pre-clinical assessment in a rabbit model of liver cancer. *Clin Cancer Res*. 2006; 12: 2563-7.
- Geschwind JF, Ko YH, Torbenson MS, Magee C, Pedersen PL. Novel therapy for liver cancer: direct intraarterial injection of a potent inhibitor of ATP production. *Cancer Res*. 2002; 62: 3909-13.
- Lewis AL, Gonzalez MV, Leppard SW, Brown JE, Stratford PW, Phillips GJ, et al. Doxorubicin eluting beads - I: effects of drug loading on bead characteristics and drug distribution. *J Mater Sci Mater Med*. 2007; 18: 1691-9.
- Mahnken AH, Pereira PL, de Baere T. Interventional oncologic approaches to liver metastases. *Radiology*. 2013; 266: 407-30.
- Choe DH, Han MH, Kang GH, Yeon KM, Han MC. An experimental study of embolic effect according to infusion rate and concentration of suspension in transarterial particulate embolization. *Invest Radiol*. 1997; 32: 260-7.